doi:10.1093/jmcb/mjy024
Published online April 6, 2018

Article

EMC10 governs male fertility via maintaining sperm ion balance

Yuchuan Zhou[1], Fei Wu[2], Man Zhang[3], Zuquan Xiong[2], Qianqian Yin[1], Yanfei Ru[1], Huijuan Shi[4], Jinsong Li[3], Shanhua Mao[2], Yanliang Li[5], Xinyi Cao[5], Renming Hu[5], Chong Wee Liew[6], Qiang Ding[2,*], Xuanchun Wang[5,*], and Yonglian Zhang[1,*]

[1] State Key Laboratory of Molecular Biology, Shanghai Key Laboratory of Molecular Andrology, CAS Center for Excellence in Molecular Cell Science, Shanghai Institute of Biochemistry and Cell Biology, Chinese Academy of Sciences, University of Chinese Academy of Sciences, Shanghai 200031, China
[2] Department of Urology, Huashan Hospital, Fudan University, Shanghai 200040, China
[3] State Key Laboratory of Cell Biology, Shanghai Key Laboratory of Molecular Andrology, CAS Center for Excellence in Molecular Cell Science, Shanghai Institute of Biochemistry and Cell Biology, Chinese Academy of Sciences, University of Chinese Academy of Sciences, Shanghai 200031, China
[4] China National Population and Family Planning Key Laboratory of Contraceptive Drugs and Devices, Shanghai Institute of Planned Parenthood Research, Shanghai 200030, China
[5] Department of Endocrinology, Huashan Hospital, Fudan University, Shanghai 200040, China
[6] Department of Physiology & Biophysics, College of Medicine, University of Illinois at Chicago, Chicago, IL 60612, USA
* Correspondence to: Qiang Ding, E-mail: dr_dingqiang@hotmail.com; Xuanchun Wang, E-mail: wangxch@fudan.edu.cn; Yonglian Zhang, E-mail: ylzhang@sibcb.ac.cn

Edited by Xuebiao Yao

Infertility is a severe public health problem worldwide that prevails up to 15% in reproductive-age couples, and male infertility accounts for half of total infertility. Studies on genetically modified animal models have identified lots of genes involved in the pathogenesis of male infertility. The underlying causes, however, remain largely unclear. In this study, we provide evidence that EMC10, one subunit of endoplasmic reticulum (ER) membrane protein complex (EMC), is required for male fertility. EMC10 is significantly decreased in spermatozoa from patients with asthenozoospermia and positively associated with human sperm motility. Male mice lacking *Emc10* gene are completely sterile. *Emc10*-null spermatozoa exhibit multiple defects including abnormal morphology, decreased motility, impaired capacitation, and impotency of acrosome reaction, thereby which are incapable of fertilizing intact or ZP-free oocytes. However, intracytoplasmic sperm injection could rescue this defect caused by EMC10 deletion. Mechanistically, EMC10 deficiency leads to inactivation of Na/K-ATPase, in turn giving rise to an increased level of intracellular Na^+ in spermatozoa, which contributes to decreased sperm motility and abnormal morphology. Other mechanistic investigations demonstrate that the absence of EMC10 results in a reduction of HCO_3^- entry and subsequent decreases of both cAMP-dependent protein kinase A substrate phosphorylation and protein tyrosine phosphorylation. These data demonstrate that EMC10 is indispensable to male fertility via maintaining sperm ion balance of Na^+ and HCO_3^-, and also suggest that EMC10 is a promising biomarker for male fertility and a potential pharmaceutical target to treat male infertility.

Keywords: *Emc10* knockout, sperm maturation, male infertility, ion imbalance, Na/K-ATPase

Introduction

The endoplasmic reticulum (ER)–membrane protein complex (EMC) was first discovered in yeast as a six-subunit (Emc1–6) transmembrane protein complex for protein folding in the ER (Jonikas et al., 2009). Later, proteomic work on studying ER-associated degradation showed the involvement of 10 subunits (EMC1–10) in animals (Christianson et al., 2011). EMC is a multifunctional and evolutionarily conserved protein complex. It has been implicated to have multiple roles in ER-associated degradation, ER-mitochondria tethering, and proper assembly of multi-pass transmembrane proteins. For instance, it has been postulated that EMC6 modulates ER-associated degradation of specific proteins in *Caenorhabditis elegans* and regulates cell autophagy in humans (Li et al., 2013; Richard et al., 2013). Recently, EMC has been indicated to be an ER-mitochondria tether and involved in the proper assembly of multi-pass transmembrane proteins (Lahiri et al., 2014; Satoh et al., 2015). In addition, EMC1 has been identified to be related to global

Received October 23, 2017. Revised January 23, 2018. Accepted April 5, 2018.

developmental delay, hypotonia, scoliosis, and cerebellar atrophy (Harel et al., 2016). Although these observations enhance our understanding of EMC biology, the functional role of EMC remains largely to be elucidated.

EMC10, as one of the EMC subunits, is an evolutionarily highly conserved gene across numerous species including plants, invertebrates, and mammals. Our group for the first time cloned this gene from a human insulinoma cDNA library, which was then named as INM02 (Wang et al., 2004, 2009). Since no homology to any known proteins or protein domains was characterized, EMC10 was thought to be a truly novel protein. To date, a number of studies have unmasked some aspects of the biological functions of EMC10. In our previous study, it was found that EMC10 (INM02) was a secreted protein which can be detected in human serum by ELISA, and murine *Emc10* gene was regulated by glucose in pancreatic beta cells, suggesting its role in the regulation of glucose metabolism (Wang et al., 2009). Afterwards, another group also reported the cloning of human EMC10 from purified hematopoietic stem cell populations, where they named EMC10 as HSS1 and HSM1 for its splice variant (Junes-Gill et al., 2011). *In vitro* study indicated that EMC10 (HSS1) inhibited cell proliferation, migration, and invasion in glioma cell lines as well as angiogenesis in endothelial cells, and was proposed as a potential therapeutic target for malignant glioblastoma (Junes-Gill et al., 2011, 2014). In a mouse model with schizophrenia, elevation of Mirta22, the murine ortholog of human EMC10, inhibited dendritic and spine development (Xu et al., 2013). Reduction of Mirta22 levels, however, totally rescued the deficits in dendritic and spine formation at hippocampal pyramidal neurons of the mouse model, suggesting an important role of mouse Emc10 in the formation of neuronal dendrites and spines (Xu et al., 2013). Despite these advances, the biological role of EMC10 and the underlying mechanism remain largely unknown.

To elucidate the biological function of EMC10 *in vivo*, we generated *Emc10* knockout mouse model. During the study of phenotypes of homozygous mice, we accidentally found that male *Emc10*-deficient mice were infertile. In this report, we characterized the role of EMC10 in governing sperm maturation and male fertility, and revealed the underlying mechanism by which EMC10 regulated the sperm functions. By measuring EMC10 expression in spermatozoa collected from asthenozoospermic patients and controls, we also investigated the clinical relevance of EMC10 with sperm motility and male fertility.

Results

Emc10 gene deletion leads to male infertility in mice

To address the uncharacterized biological function of EMC10, we established *Emc10* knockout mice by disrupting the second exon of *Emc10* gene to suppress *Emc10* expression (Supplementary Figure S1). *Emc10* knockout ($Emc10^{-/-}$) mice were indistinguishable from their wild-type ($Emc10^{+/+}$) littermates in survival rates, appearance, and gross behavior. Importantly, it was observed that $Emc10^{-/-}$ male mice were completely infertile (Figure 1A), and the female mice exhibited reduced fertility (data not shown). Mating of six *Emc10*-null males with varied numbers of wild-type females over a period of 3 months still yielded no offspring, even though

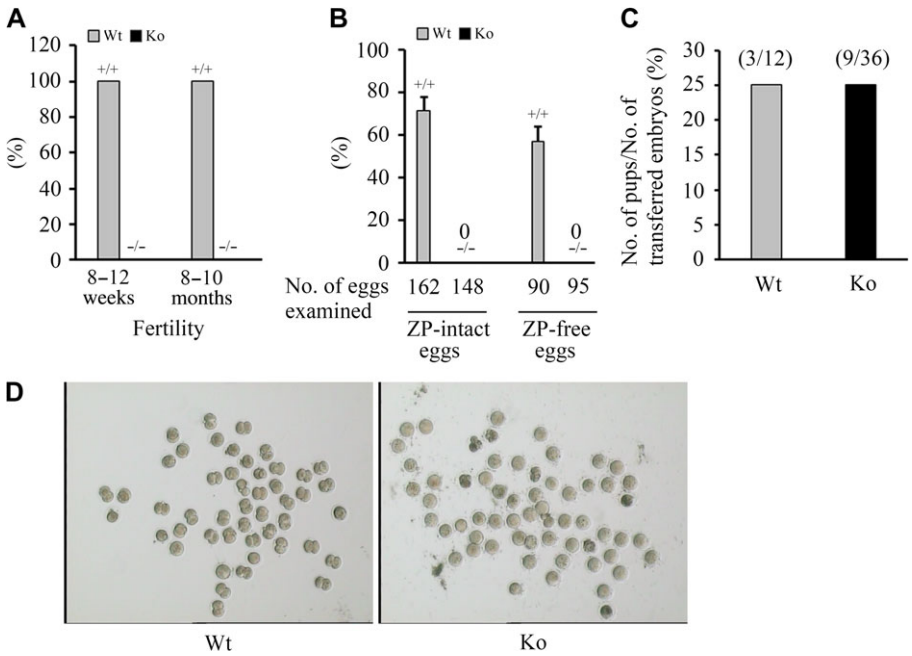

Figure 1 Effect of *Emc10* disruption on male fertility. (**A**) Fertility of $Emc10^{+/+}$ (Wt) and $Emc10^{-/-}$ (Ko) male mice (n = 18). (**B**) Analysis of *in vitro* fertilization of spermatozoa from Wt and Ko mice with intact and ZP-free oocytes, respectively (n = 3). Data are presented as mean ± SEM. (**C**) Analysis of the fertilizing ability after ICSI with spermatozoa from Wt and Ko mice. (**D**) Images of *in vitro* fertilization showing oocytes and two-cell embryos.

seminal plugs, indicative of normal copulation, were present in the female reproductive tract.

To confirm the phenotype of male infertility, *in vitro* fertilization assay was performed to determine the ratio of two-cell embryos to the total number of inseminated oocytes. The results showed that none of intact oocytes incubated with *Emc10*$^{-/-}$ sperm cells was able to develop to two-cell stage (Figure 1B and D). To examine whether the *Emc10*-deficient spermatozoa retained the ability to fuse with the plasma membrane and activate fertilization, we incubated *Emc10*$^{-/-}$ spermatozoa with ZP-free oocytes. It turned out that *Emc10*$^{-/-}$ spermatozoa was also incapable of fertilizing ZP-free oocytes (Figure 1B). However, intracytoplasmic sperm injection (ICSI) by which *Emc10*$^{-/-}$ spermatozoa were inserted directly into the cytoplasm of wild-type oocytes can reverse the male infertility, evidenced by the observation that *Emc10*$^{-/-}$ spermatozoa-injected oocytes which were transplanted into the oviducts of pseudo-pregnant females successfully developed into normal embryos (Figure 1C). Taken together, these data demonstrate that the *Emc10*-null spermatozoon carries an intact haploid genome as a result of normal spermatogenesis, and also suggest that EMC10 is involved in the interaction of spermatozoa with oocytes.

EMC10 disruption impairs sperm functions

The overall body weights of the *Emc10*-null male mice were not different from those of wild-type animals (Supplementary Figure S2A). The testicular weight and epididymal sperm count from *Emc10* knockout mice were statistically decreased at the age of 8–12 weeks compared with wild-type. Differences in the parameters above, however, disappeared when mice grew up to 8–10 months (Supplementary Figure S2B and C). If normalized by testis weight, the sperm count did not exhibit differences any more between wild-type and homozygous mice at any age (Supplementary Figure S2D). Additionally, the weight of epididymis as well as the morphologies of both testes and epididymis did not display overt aberrations in homozygous mice compared with wild-type (Supplementary Figure S2E–G). These data suggest that the deficit of *Emc10* does not affect spermatogenesis, nor does influence the development of testis and epididymis.

After leaving from the testis, spermatozoa must undergo functional maturation in the epididymis before they can competently interact with oocytes (Orgebin-Crist, 1967). This process includes the acquisition of sperm motility and the potential for sperm capacitation as well as undergoing the acrosome reaction. To elucidate the defects underlying the male fertility, we collected and incubated epididymal spermatozoa in capacitating medium and examined the parameters of sperm motility every 30 min for 2 h at room temperature by employing a computer-assisted sperm analysis. The results indicated that EMC10 deficiency significantly decreased the sperm motility including the main motility parameters of total motility (Figure 2A), path velocities (Figure 2B), linear velocities (Figure 2C), and track velocities (Figure 2D). Sperm viability was similar between *Emc10*-null and wild-type mice (94.0% ± 1.0% vs. 93.7% ± 1.1%, respectively). This finding indicates that the lower motility in the *Emc10*-null mice was not caused by sperm death, which was confirmed by the similar response to external calcium ions in the *Emc10*$^{+/+}$ and *Emc10*$^{-/-}$ sperm cells (Figure 6E). The normal capacitation of mouse cauda epididymidal spermatozoa *in vitro* was registered as a time-dependent increase in protein tyrosine phosphorylation of a subset of proteins (Visconti et al., 1995a). However, when *Emc10*$^{-/-}$ spermatozoa were capacitated *in vitro*, the time-dependent rise of capacitation-associated protein tyrosine phosphorylation was almost abolished (Figure 2E). The serine/threonine phosphorylation of PKA substrate proteins is a critical event on the upstream of sperm capacitation-associated protein tyrosine phosphorylation (Baker et al., 2006). We investigated PKA substrate phosphorylation in sperm and observed that EMC10 deficiency resulted in a decrease of PKA substrate phosphorylation (Figure 2F), which is consistent with the reduction of tyrosine phosphorylation in *Emc10*$^{-/-}$ sperm. Furthermore, CTC staining was performed to assess the acrosome reaction based on the alteration of staining patterns of the sperm head with F pattern representing for uncapacitated cells, B pattern for capacitated cells, and AR pattern for acrosome-reacted spermatozoa (Xu et al., 2007). The results revealed a significant increase in the percentage of uncapacitated spermatozoa (F pattern) in the *Emc10*-null group (Figure 2G). On the contrary, the percentage of capacitated cells (B pattern) was significantly reduced in the null mice (Figure 2G), indicating that the sperm capacitation was inhibited and confirming the observation of the decreased capacitation-associated protein tyrosine phosphorylation in the *Emc10*-null mice (Figure 2E). The percentage of spontaneous acrosome-reacted spermatozoa (AR pattern) was also significantly decreased in *Emc10*$^{-/-}$ mice (Figure 2G). Moreover, *Emc10*$^{-/-}$ spermatozoa lost the ability to respond to A23187 or progesterone, reagents to induce acrosome reaction (Figure 2H). Collectively, these observations indicate an essential role of EMC10 in sperm maturation in the epididymis.

In addition, the spatial distribution of EMC10 in spermatozoon provided hints for the study on the function of EMC10. Immunofluorescence analysis showed that EMC10 was confined to the principal piece domain on testicular spermatozoa, but underwent relocation from the midpiece to the head during epididymal transit (Figure 3A). In humans, EMC10 was localized at the acrosome region of ejaculated spermatozoa (Figure 3B). The immunofluorescent data also indicated that EMC10 and PNA-FITC signals, indicators of the acrosome, co-existed in mouse and human spermatozoa (Figure 3C). These distinct cellular locations of EMC10 in spermatozoa from different epididymal regions imply that EMC10 is involved in multiple aspects of sperm function in the epididymis.

Spermatozoa from Emc10-null mice exhibit abnormal morphology

Morphological analysis of spermatozoa from the testis and different regions of the epididymis revealed that the hairpin phenotype appeared gradually in the *Emc10*$^{-/-}$ spermatozoa, when compared with the spermatozoa from wild-type mice (Figure 4). There was no difference in morphology between the *Emc10*-null and wild-type spermatozoa obtained from the testis

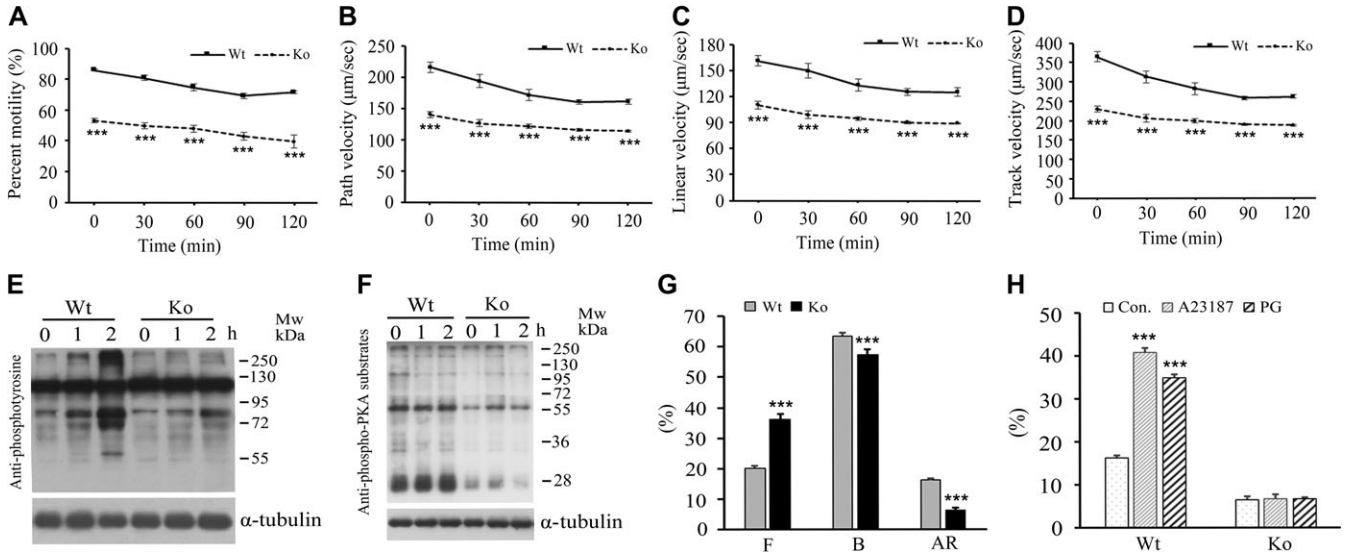

Figure 2 Effect of *Emc10* disruption on sperm function. (**A**) The percentage of motile spermatozoa from wild-type (Wt) and *Emc10*-null (Ko) mice during 2-h incubation in medium ($n = 4$). (**B**–**D**) Comparison of path velocity (**B**), linear velocity (**C**), and track velocity (**D**) of spermatozoa from Wt and Ko mice ($n = 4$). (**E** and **F**) Measurement of capacitation-associated protein tyrosine phosphorylation (**E**) and PKA substrate phosphorylation (**F**) of spermatozoa from Wt and Ko mice. Spermatozoa were incubated in capacitating medium and collected for western blot per hour. α-tubulin served as the loading control. The western blot is representative of four independent experiments. (**G**) The percentage of uncapacitated (F pattern), capacitated (B pattern), and acrosome-reacted (AR pattern) spermatozoa from Wt and Ko mice. (**H**) Examination of the acrosome reaction induced by A23187 or progesterone in sperm from Wt and Ko mice ($n = 7$). Data are presented as mean ± SEM. ***$P < 0.001$ when compared with respective controls.

(Figure 4A). However, spermatozoa isolated from the caput and proximal corpus epididymidis of *Emc10*$^{-/-}$ mice displayed a sharp bend at the junction between midpiece and principal piece (Figure 4B and C). Moreover, many *Emc10*$^{-/-}$ sperm tails showed hairpin bending at the annulus when they arrived at the distal corpus and cauda epididymidis (Figure 4D and E). By the time spermatozoa reached the cauda epididymidis, 56% displayed this morphological hairpin bending (Figure 4F). These results show that deficiency of EMC10 leads to structural abnormality in mouse sperm, and also suggest that EMC10 is essential for the maintenance of normal sperm morphology during the transit through the epididymis.

Emc10-null spermatozoa exhibit a dramatically altered proteomic expression profile

Next, we sought to explore the underlying mechanism of the sperm dysfunction caused by EMC10 deficiency. Since the transcription is silent in mature sperm cells, we performed an unbiased screening analysis on the proteome-wide scale by using a Tandem Mass Tag (TMT)-labeled quantitative technique (Thompson et al., 2003). Seventeen wild-type and 17 *Emc10*-deficient male mice were included and randomly assigned to six groups, as illustrated in the workflow diagram in Supplementary Figure S3. The proteomic analyses were performed in triplicate, by using a quadrupole-Orbitrap mass spectrometer (Q-Exactive), and the data processing and quantification were done by Mascot and Scaffold Q+. Notably, out of 4351 identified proteins, 327 proteins were found to be altered significantly with >1.5-fold expression in *Emc10*-null spermatozoa in comparison with wild-type (Supplementary Table S1). Strikingly, the heat map and volcano plots of 327 significantly changed proteins showed that 96.6% (316/327) of the identified proteins were upregulated, only 3.4% (11/327) were downregulated in the *Emc10*$^{-/-}$ sperm cells (Figure 5A and B). By using the DAVID website (http://david.abcc.ncifcrf.gov/), these 327 target proteins were analyzed to identify the gene ontology (GO) biological processes which were significantly altered in *Emc10*-deficient spermatozoa. R-Script diagram indicated that the top five biological processes significantly changed in *Emc10*$^{-/-}$ spermatozoa (Figure 5C) were translation, translational initiation, cilium morphogenesis, spermatogenesis, and cilium assembly. In addition, pathway enrichment analysis by ingenuity pathway analysis (IPA) showed that EIF2 and PI3K/Akt signaling pathways were significantly activated, while eNOS pathway was significantly inhibited (Figure 5D). Work module analysis by IPA showed that the deletion of EMC10 led to the upregulation of a set of proteins involved in the promotion of fertility and the inhibition of sperm disorder and cell death of germ cells, both of which should give rise to enhanced male fertility (Figure 5E). Clusters of proteins associated with the inhibition of cell death or apoptosis were also found upregulated in *Emc10*-null spermatozoa, suggesting that EMC10 deficiency results in increased cell survival (Supplementary Figure S4). Theoretically, both activation of fertility and increase of cell survival are favorable to male fertility in *Emc10*-deficiency mice. Therefore, these observations are incompatible with the

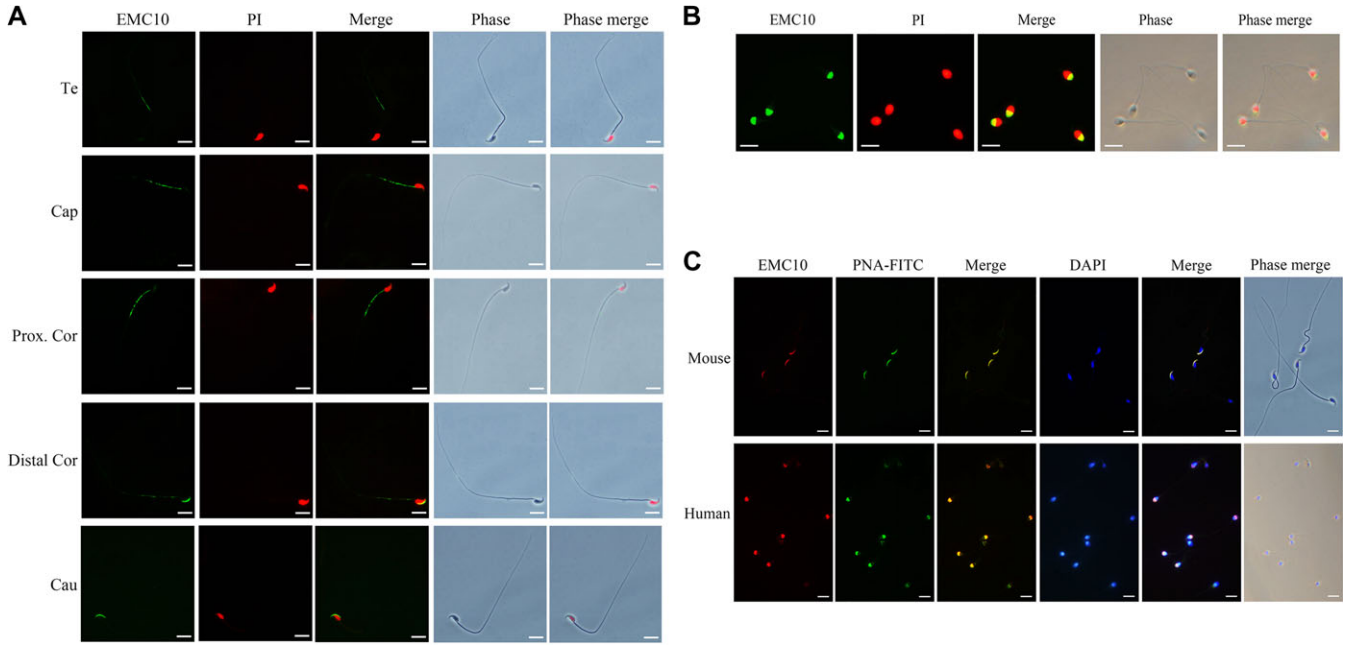

Figure 3 The spatial distribution of EMC10 in mouse and human spermatozoon. (**A**) Immunostaining of EMC10 protein (green) on mouse spermatozoa from testis and different regions of the epididymis. Te, testis; Cap, caput epididymidis; Prox.Cor, proximal corpus epididymidis; Distal.Cor, distal corpus epididymidis; Cau, cauda epididymidis. (**B**) Immunostaining of EMC10 (green) on human spermatozoa. Nuclei were labeled with PI (red). (**C**) Immunofluorescent analysis of the localization of EMC10 protein (red) and the acrosome marker PNA-FITC (green) demonstrating the cellular localization of EMC10 in the acrosomal domain of spermatozoa from wild-type mice and humans. Nuclei were labeled with DAPI (blue). Scale bar, 10 μm.

sterile phenotype of *Emc10*-null mice. To figure out the molecular mechanism underlying the male infertility, we decided to focus on the downregulated proteins to explore the driving force of sperm dysfunction upon EMC10 deficiency. Very few proteins were detected with significant downregulation in *Emc10*-deficient sperm, among which ATP1B3 and ATP1A4, the Na/K-ATPase subunits, were the only two proteins whose expressions were decreased by >3-fold in *Emc10*-null spermatozoa compared with wild-type (Figure 5B). This finding strongly suggests that EMC10 exerts an important impact on the regulation of the activity of Na/K-ATPase.

EMC10 knockout causes ion imbalance in spermatozoa

The Na/K-ATPase enzyme plays a critical role in maintaining the low intracellular Na^+ concentration (Kaplan, 2002). Proteomic data showed that ATP1A4 and ATP1B3, the α and β subunits of Na/K-ATPase, were the two most downregulated proteins in the *Emc10*-null spermatozoa (Figure 5B), which was subsequently validated by western blotting showing that the two proteins were almost deleted in null spermatozoa (Figure 6A and B). We also checked the protein levels of both ATP1B3 and ATP1A4 in testis tissues and found that they were almost gone in the *Emc10*$^{-/-}$ testis (Supplementary Figure S5A), suggesting that EMC10 regulates the expression of these two subunits of Na/K-ATPase at the testis level. The expression of another subunit of Na/K-ATPase, ATP1A1, was also measured and no difference in its expression was observed between wild-type and null spermatozoa (Figure 6A). Afterwards, we loaded the sperm with SBFI-AM, a Na-sensitive dye, for the measurement of the Na^+ level in the sperm cytosol. The result showed that *Emc10*-null spermatozoa had significantly higher intracellular Na^+ level than the wild-type (Figure 6C). It is widely accepted that both Ca^{2+} and HCO_3^- are important for the induction of the acrosome reaction as well as hyperactivation and capacitation. Thus, sperm intracellular Ca^{2+} levels and HCO_3^--induced pH alteration were investigated. There was no significant difference in the intracellular pH between *Emc10*-null and wild-type spermatozoa incubated in HCO_3^- free medium (Figure 6D). However, the HCO_3^--induced increase in intracellular pH was significantly inhibited in *Emc10*$^{-/-}$ sperm cells either before or after 1 h of capacitation (Figure 6D). These data suggest that EMC10 is involved in the transport of HCO_3^-. A previous study showed that CFTR is involved in mediating the HCO_3^- entry during sperm capacitation (Xu et al., 2007). So we attempted to figure out whether EMC10 regulates HCO_3^- entry through CFTR. Western blot analysis showed that the expression level of CFTR protein was not different between *Emc10*$^{-/-}$ and wild-type sperm (Supplementary Figure S5B), suggesting that the EMC10-regulation of HCO_3^- entry into sperm cell is independent of CFTR pathway. As shown in Figure 6E, the Ca^{2+} level of *Emc10*$^{-/-}$ spermatozoa was not significantly different from that of wild-type in either Ca^{2+}-free medium or Ca^{2+}-containing medium, suggesting that the defect of acrosome reaction in *Emc10*-null spermatozoon was not attributable to cytosolic calcium. A previous report has demonstrated that cAMP

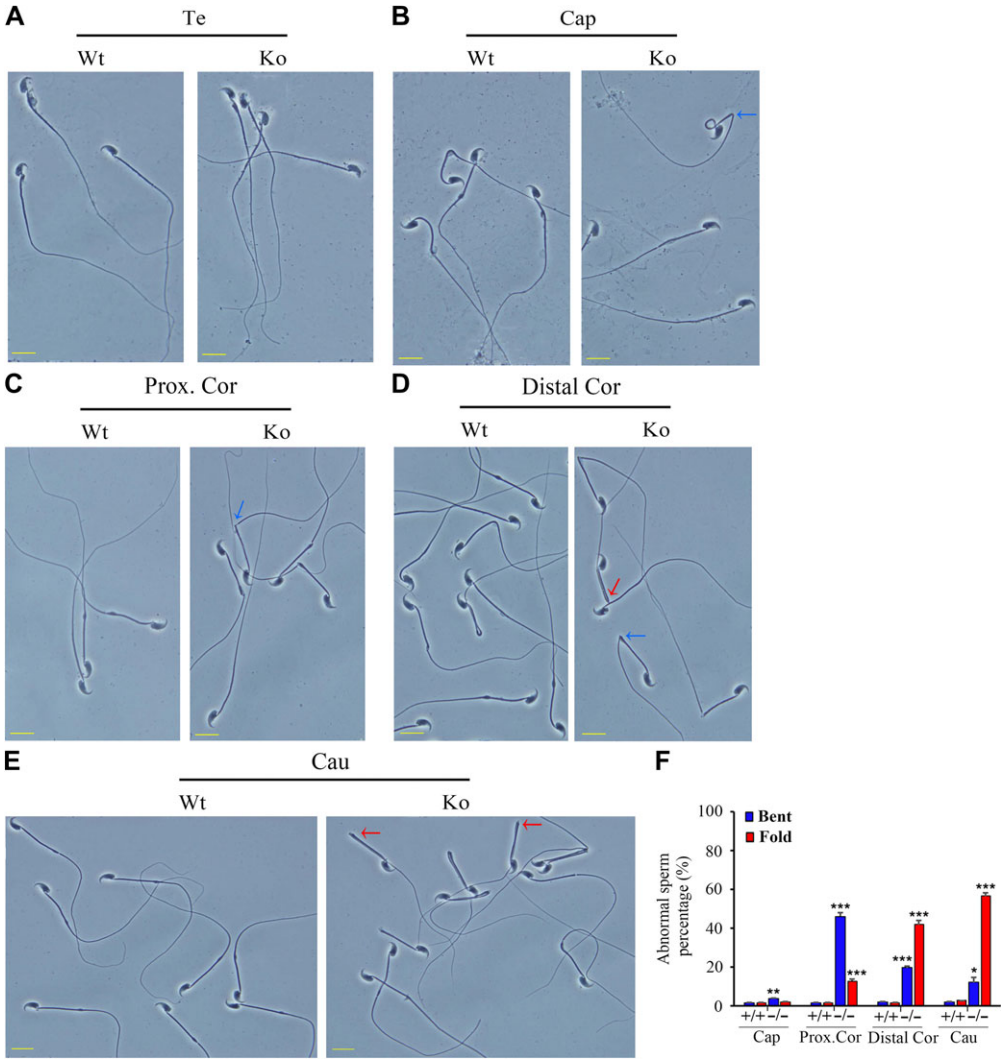

Figure 4 Morphological defects of *Emc10*$^{-/-}$ spermatozoa. (**A**–**E**) Phase contrast images of spermatozoa collected from the testis (**A**), caput (**B**), proximal corpus (**C**), distal corpus epididymidis (**D**), and cauda epididymidis (**E**) from wild-type (Wt) and *Emc10*-null (Ko) mice. Scale bar, 10 μm. (**F**) Quantification analysis of sperm with abnormal structure in different parts of the epididymis from Wt and Ko mice (n = 3). Data are presented as mean ± SEM, *$P < 0.05$, **$P < 0.01$, and ***$P < 0.001$ compared with respective controls. Te, testis; Cap, caput; Prox.Cor, proximal corpus; Distal.Cor, distal corpus; Cau, cauda epididymidis. Blue arrow, spermatozoa with bent tails; red arrow, spermatozoa with fold tails.

can rescue tyrosine phosphorylation of spermatozoa incubated in a medium devoid of HCO_3^- (Visconti et al., 1995b). To test whether the reduction of protein tyrosine phosphorylation of *Emc10*$^{-/-}$ spermatozoa was due to the defect of HCO_3^--induced cAMP increase and subsequent tyrosine phosphorylation, *Emc10*$^{-/-}$ sperm cells were incubated in capacitating medium with 8-Bromo-cAMP, a biologically active cyclic AMP (cAMP) analog, or IBMX, a cyclic nucleotide phosphodiesterase inhibitor which prevents cAMP from being hydrolyzed by cyclic nucleotide phosphodiesterases. The time-dependent increase of protein tyrosine phosphorylation in *Emc10*$^{-/-}$ sperm was completely rescued by the addition of 8-Bromo-cAMP or IBMX (Figure 6F). However, neither 8-Bromo-cAMP nor IBMX was able to recover the motility and acrosome reaction of *Emc10*$^{-/-}$ spermatozoa (Supplementary Figure S6). Taken together, these data imply that EMC10 plays an essential role in maintaining sperm ion balance of Na^+ and HCO_3^-.

Sperm EMC10 levels are positively associated with sperm motility in human

Based upon the observation on the mouse model, there is no doubt that EMC10 plays a critical role in male fertility. To figure out the role of EMC10 in human fertility, we collected semen from asthenozoospermic patients and control males, and then categorized these samples into two groups including low- and normal-motile spermatozoa. It can be seen that except motility, there were no significant differences in all other parameters between

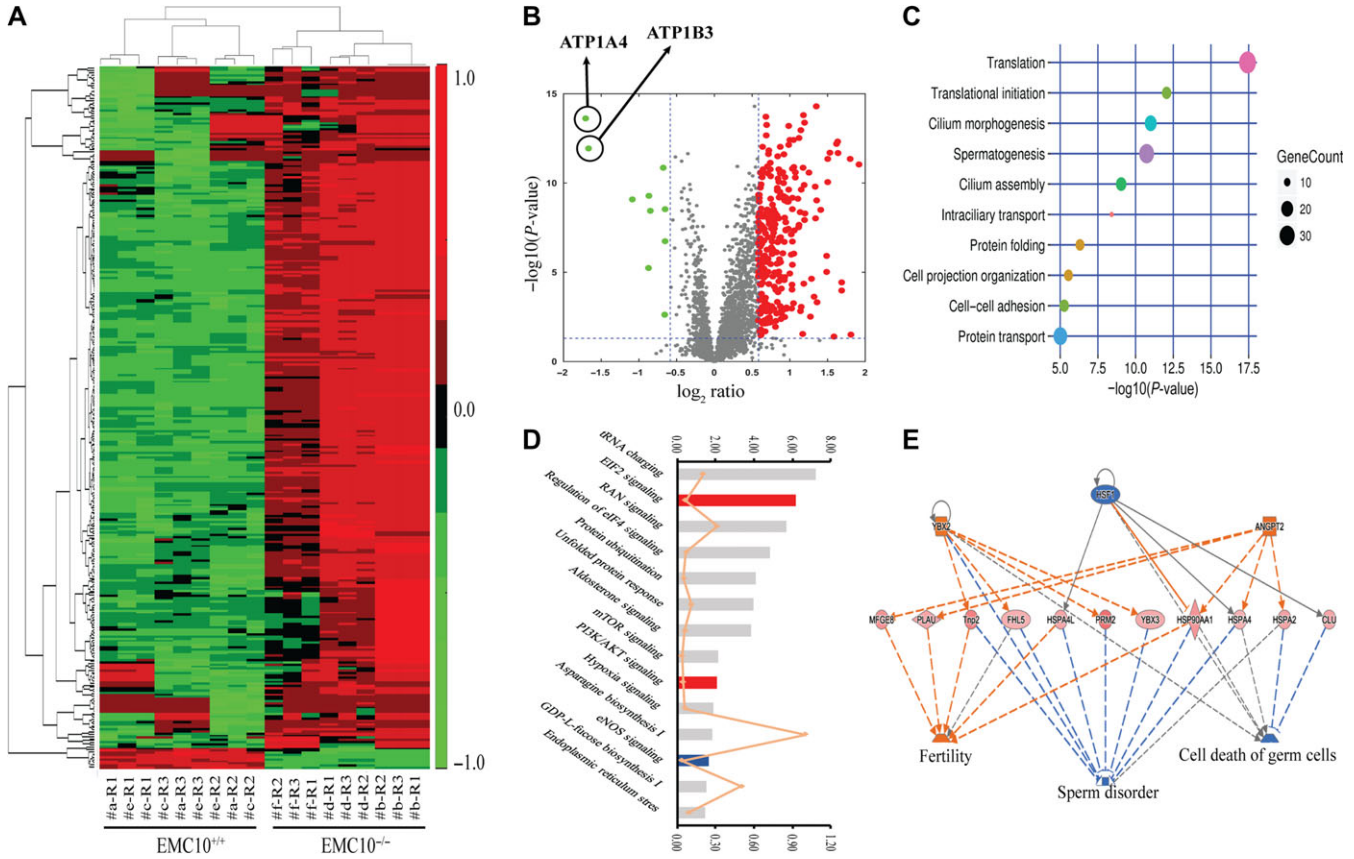

Figure 5 Proteomic analysis on the spermatozoa from wild-type and *Emc10*-null mice. (**A**) Heat map of 327 significantly increased or decreased proteins (>1.5-fold) in the spermatozoa of wild-type ($Emc10^{+/+}$) and $Emc10^{-/-}$ mice. Red represents for the upregulated proteins and green for the downregulated proteins. Values were normalized to log2-fold difference. The false discovery rate is <0.10. (**B**) Volcano plot of 327 significantly altered proteins (>1.5-fold) in the spermatozoa of $Emc10^{-/-}$ mice compared with wild-type controls. Red, upregulation; green, downregulation. (**C**) GO term enrichment analysis. The 327 significantly changed proteins were analyzed to identify the GO biological processes from the DAVID website (http://david.abcc.ncifcrf.gov/). A R-Script diagram was generated to visualize the top 10 significantly altered biological processes in $Emc10^{-/-}$ spermatozoa. (**D**) Distribution of top 14 enriched pathways in the filtered data set of detected proteins according to the analysis by IPA (www.ingenuity.com). Fisher's test was applied and proteins with >1.5-fold change in abundance were included. The top coordinates are –log10-transformed *P*-values. The bottom coordinates are the ratio of differentially expressed proteins and the number of proteins in the indicated pathway. Red, pathways were predicted to be significantly activated; blue, pathways predicted to be significantly downregulated; gray, pathways without predicted results. (**E**) The predicted work modules based on the 327 significantly altered proteins (>1.5-fold) in the sperm of $Emc10^{-/-}$ mice. Orange labeling indicates increased measurement (e.g. YBX2, ANGPT2) or the effect predicted to be activated (e.g. fertility), while blue characters represent decreased measurement (e.g. HSF1) or the effect predicted to be inhibited (e.g. sperm disorder, cell death of germ cells). The dashed lines indicate the predicted interactions between network proteins, and the directions of the interaction are indicated by orange arrows (activation), blue-blocked lines (inhibition), or gray lines (effect not predicted).

the two group including age, semen volume, sperm count, and sperm morphology (Table 1). The EMC10 protein levels in spermatozoa from these samples were subsequently measured by using western blotting (Figure 7A). The scatter diagram showed that the protein levels of EMC10 appeared to be positively associated with the sperm motility (Figure 7B). Accordingly, statistical analysis indicated that low-motile spermatozoa (A + B < 50%) had significantly reduced levels of EMC10, compared with normal-motile spermatozoa (A + B > 50%) (Figure 7C, $P < 0.01$). Taken together, these results demonstrate that EMC10 is involved in the regulation of human sperm motility, and also suggest that low sperm EMC10 is a causative factor for male infertility in human.

We have shown that EMC10 deletion led to the loss of ATP1A4 in mouse sperm. It was reported that *Atp1a4* knockout mice were completely sterile and exhibited the similar phenotypes as *Emc10*-null mice (Jimenez et al., 2011). We try to investigate whether ATP1A4 is associated with male infertility or reduced sperm motility in human. Twelve human sperm samples from patients with asthenozoospermia and control male were collected and their motility and ATP1A4 expression were measured (Figure 7D). Correlative

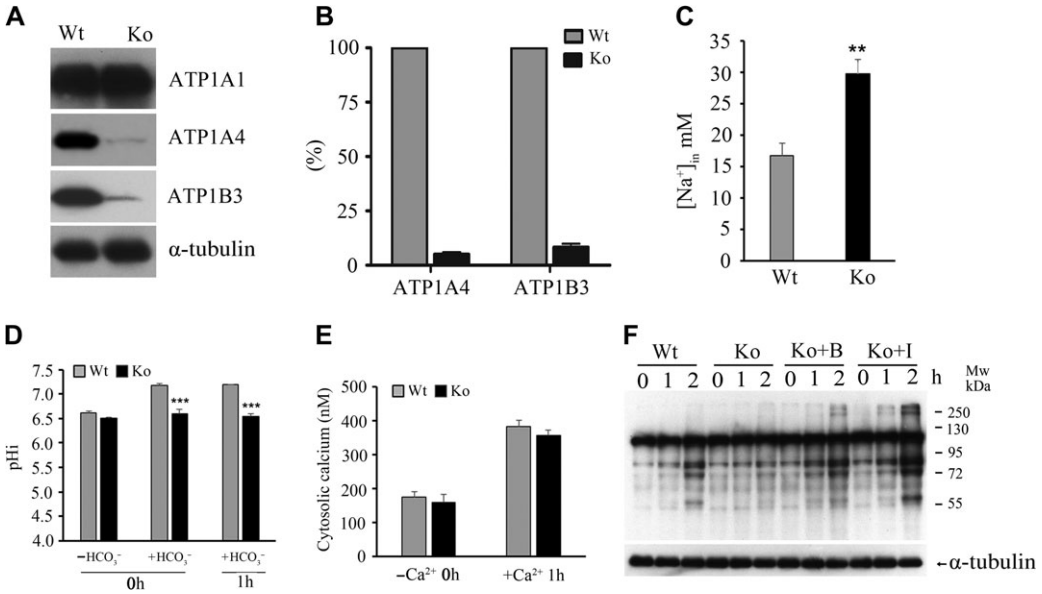

Figure 6 Effect of *Emc10* deletion on ATPase expression and ionic equilibrium in spermatozoa. (**A**) Determination of ATP1A1, ATP1A4, and ATP1B3 protein levels in spermatozoa from wild-type (Wt) and *Emc10*-null (Ko) mice. α-tubulin was used as the protein loading control. The western blot shows a representative result of six independent experiments. (**B**) Quantitative analysis of ATP1A4 and ATP1B3 protein levels based on densitometry of western blot in **A**. (**C**) Intracellular Na^+ concentration in spermatozoa from Wt and Ko mice. (**D**) Determination of intracellular pH in Wt and Ko spermatozoa incubated in HCO_3^--free medium or HCO_3^--containing medium for 0 or 1 h. (**E**) Determination of intracellular Ca^{2+} in Wt and Ko spermatozoa incubated in Ca^{2+}-free or Ca^{2+}-containing medium. (**F**) Detection of capacitation-associated protein tyrosine phosphorylation of Ko spermatozoa incubated in capacitating medium in the presence of 1 mM 8-Bromo-cAMP or 100 μM IBMX. A representative western blot of four independent experiments is shown. α-tubulin was used as the protein loading control. B, 8-Bromo-cAMP; I, IBMX. Data are presented as mean ± SEM, $n = 4$, $^{**}P < 0.01$, $^{***}P < 0.001$, when compared with control.

Table 1 Characteristic parameters of the clinical spermatozoon samples.

	Low-motile spermatozoa	Normal-motile spermatozoa	*P*-value
Number	20	7	
Age (year)	30.45 ± 3.29	29.57 ± 4.47	0.601
Semen (ml)	4.63 ± 1.73	4.00 ± 1.07	0.396
Survival ratio (%)	55.50 ± 8.65	62.14 ± 9.20	0.110
Grade A (%)	12.25 ± 5.80	23.57 ± 2.26	<0.001
Grade B (%)	17.75 ± 3.70	30.00 ± 0.00	<0.001
Motile			
Spermatozoa (A% + B%)	30.00 ± 8.51	53.57 ± 2.26	<0.001
Grade C (%)	23.00 ± 6.96	17.14 ± 2.47	0.046
Grade D (%)	47.00 ± 6.40	29.29 ± 1.75	<0.001
Sperm count (10^6)	55.88 ± 26.81	70.14 ± 30.10	0.270
Morphologically normal ratio (%)	53.00 ± 6.40	58.57 ± 6.39	0.068
EMC10 protein levels	0.18 ± 0.30	0.65 ± 0.38	0.004

A + B ≥ 50% was considered as normal-motile spermatozoa, and A + B < 50% was considered as low-motile spermatozoa.

analysis showed that the levels of ATP1A4 are positively associated with sperm motility (Figure 7E), which is consistent with the association between EMC10 expression and sperm motility. These data imply that ATP1A4 is involved in the EMC10-regulated male fertility in human.

Discussion

Several previous studies have explored the biological function of EMC10 in mammalian cells (Wang et al., 2009; Junes-Gill et al., 2011, 2014; Xu et al., 2013). However, they did not directly illustrate the physiological role of EMC10 *in vivo*. Our present study for the first time characterized the essential role of EMC10 in male fertility by using *Emc10* knockout mouse model. Our data revealed multiple defects of *Emc10*$^{-/-}$ spermatozoa including structural abnormality, impaired capacitation, decreased motility, and impotency of acrosome reaction, which together led to male infertility.

Since no homology to any known protein domains was found in EMC10, we tried to dissect the molecular mechanism underlying EMC10 deficiency-caused infertility by using proteomic analysis. Surprisingly, it turned out that deletion of EMC10 led to the upregulation of a set of proteins involved in enhancing male fertility, which we proposed as a compensatory response to the infertility. The compensation, however, still did not rescue the sterility, which highlighted the indispensable role of EMC10 in male fertility. On the other hand, it is reasonable to speculate that the male sterility is driven by downregulated Na/K-ATPase subunit proteins ATP1B3 and ATP1A4. Na/K-ATPase consists of a catalytic α-subunit and a glycosylated β-subunit. The β-subunit can stabilize the newly synthesized α-subunit, and only the α-subunit assembled with the β-subunit can be targeted to the plasma membrane where Na/K-ATPase mediates active transport (Ueno et al., 1997). In addition, the β-subunit might directly affect catalytic activation (Ueno et al., 1997). It is well known that Na/K-ATPase is responsible for maintaining the low intracellular

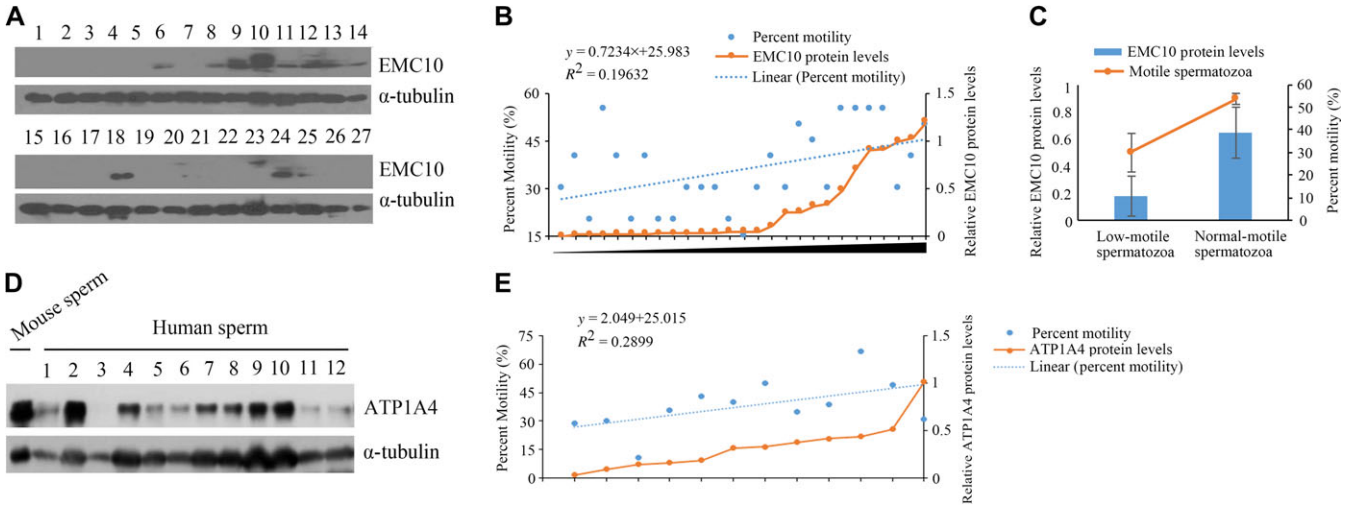

Figure 7 The correlation of EMC10 or ATP1A4 protein level with sperm motility in humans. (**A**, **B**, **D**, and **E**) Immunoblot (IB) analysis was performed to determine the levels of EMC10 (**A**) and ATP1A4 (**D**) in sperm protein derived from asthenozoospermic patients and male controls. The scatter diagram shows the motile spermatozoa percentage and the relative protein levels of EMC10 (**B**) or ATP1A4 (**E**). The percentage of motile spermatozoa was quantified by ImageJ software (v2.1). The linear regression analysis was analyzed by using the Statistical Package for the Social Sciences (SPSS 20.0) software program. (**C**) The histogram shows motile sperm percentage and the relative protein levels of EMC10. Data are presented as mean ± SD, $^{**}P < 0.01$.

Na^+ concentration (Kaplan, 2002). We observed that EMC10 deficiency resulted in almost deletion of both ATP1A4 and ATP1B3, the α and β subunits of Na/K-ATPase, which in turn produced a significantly elevated Na^+ concentration in *Emc10*$^{-/-}$ spermatozoa. It was reported that ion balance and adequate intercellular Na^+ levels were required for normal sperm motility (Darszon et al., 2006). Additionally, a similar abnormality of morphology exhibited in *Emc10*$^{-/-}$ spermatozoa has been previously noted in wild-type sperm after treatment with ion channel blockers which also caused increased levels of intercellular Na^+ (Cooper et al., 2004). Collectively, it implies that both structural abnormality and low motility are due to sodium imbalance in *Emc10*-null spermatozoa. Notably, ATP1A4 knockout mice exhibited the same phenotypes shown in *Emc10*-null mice including decreased sperm motility, a complete bending of the head over the principal piece of the flagellum as well as male infertility (Jimenez et al., 2011). Accordingly, our data suggest that EMC10 plays an important role in regulating the activity of Na/K-ATPase, and therefore governing sperm membrane Na^+ transport. We propose that sperm Na^+ imbalance caused by Na/K-ATPase deficiency accounts for the mechanism underlying the male infertility in *Emc10*-null mice. To our knowledge, there is no study showing the relevance of ATP1B3 with male fertility. Here, we also provide hints for the future study investigating the impact of ATP1B3 on male fertility.

In addition to sodium imbalance, we identified a significant reduction in HCO_3^--induced pH in *Emc10*-null spermatozoa. It is well established that HCO_3^- can directly activate a HCO_3^--sensitive soluble adenylyl cyclase, which in turn stimulates cAMP production, thereby resulting in subsequent PKA activation and protein tyrosine phosphorylation (Visconti et al., 1995a). The absence of EMC10 led to a decrease of HCO_3^--induced pH and subsequent reductions of both cAMP-dependent PKA substrate phosphorylation and protein tyrosine phosphorylation, suggesting that EMC10 also plays a critical role in the transport of HCO_3^-. The fact that both 8-Bromo-cAMP and IBMX can restore protein tyrosine phosphorylation further confirmed that the impaired capacitation in *Emc10*$^{-/-}$ sperm was attributable to the defect of HCO_3^- transport. The impotency of acrosome reaction of *Emc10*$^{-/-}$ spermatozoa, however, was not overcome by 8-Bromo-cAMP or IBMX, consistent with previous reports that cAMP analogs do not completely restore the ZP-induced acrosome reaction under conditions where protein tyrosine phosphorylation appears to be completely restored (Visconti et al., 1995b). Meanwhile, neither 8-Bromo-cAMP nor IBMX could rescue the decreased motility of *Emc10*$^{-/-}$ sperm cells. This result is in keeping with previous observations that the motility and capacitation of spermatozoa are regulated by independent mechanisms in some instances (Zeng and Tulsiani, 2003; Abou-haila and Tulsiani, 2009). Based upon these observations, it suggests that the regulation of membrane HCO_3^- transport and subsequent capacitation-associated protein tyrosine phosphorylation serves as another mechanism by which EMC10 governs male fertility. However, it seems likely that the regulation of sperm motility and acrosome reaction by EMC10 is independent of HCO_3^--induced protein tyrosine phosphorylation.

Under conditions of natural fertilization, spermatozoa must penetrate the surrounding layer of the zona pellucida proteins and fuse to the oolemma. Spermatozoa with low motility are not able to penetrate intact eggs, but they are capable of fertilizing zona-pellucida-free (ZP-free) eggs (Ren et al., 2001). *Emc10*$^{-/-}$ spermatozoa with low motility could not fertilize intact or even ZP-free

oocytes, indicating that the reduced sperm motility did not completely account for the infertility caused by *Emc10* deletion. *Emc10*$^{-/-}$ spermatozoa exhibited impotency of acrosome reaction. Even though induced by A23187 or progesterone, these spermatozoa still failed to recover acrosome reaction. However, the infertility could be overcome by ICSI. Undoubtedly, the defect of acrosome reaction of *Emc10*$^{-/-}$ spermatozoa is a causative factor for the male infertility. The mechanism underlying EMC10 affects acrosome reaction, however, is still unknown, which needs further investigation in the future.

Proteomic analysis revealed that 96.6% of identified proteins were upregulated in the *Emc10*$^{-/-}$ spermatozoa, in agreement with the observation that EIF2 signaling was the most significantly activated pathway in the null spermatozoa. It is well known that EIF2 signaling plays a critical role in the control of global translation (Wek et al., 2006). In addition, GO biological process analysis showed that these identified proteins were preferentially involved in the biological processes of translation and translational initiation. It was reported that EMC10 was expressed ubiquitously in various tissues, not only limited to the testis or sperm cells. These facts demonstrate that besides maintaining male fertility, EMC10 might be of universal and fundamental significance in translational biology.

Taken together, our data demonstrate that the EMC10 is essential for male fertility via regulating sperm motility, acrosome reaction and capacitation-associated protein tyrosine phosphorylation, as well as maintaining normal sperm morphology. We also present evidence that EMC10 exerts an important impact on governing sperm ion balance of Na^+ and HCO_3^-, which is proposed as the mechanism underlying EMC10 maintains male fertility. The observation that EMC10 is decreased in spermatozoa from patients with asthenozoospermia and positively associated with human sperm motility makes EMC10 as a promising biomarker and a potential pharmaceutical target for male infertility.

Methods

Animals

Mice were housed in the Shanghai Research Center for Model Organisms before manipulation. Food and water were freely available throughout the experiments. All experimental protocols and animal experiments were approved by the Institutional Animal Care and Use Committee of the Institute of Biochemistry and Cell Biology (Permit No.: SYXK2007-0017), Shanghai Institutes for Biological Sciences, Chinese Academy of Sciences.

Generation and maintenance of Emc10 knockout mice

The gene-targeting strategy was established on the basis of the mouse genomic DNA sequence (ENSMUSG00000008140). The target vector was achieved by ET cloning (Liu et al., 2003). Two loxp elements were inserted to flank exon 2 of *Emc10* gene and a neomycin-resistant element was inserted between intron 2 and intron 3 for obtaining the targeting vector by homologous recombination in bacteria (Supplementary Figure S1A). The linearized vectors were electroporated into embryonic stem (ES) cells derived from 129 Sv/Ev mice (SCR012, Chemicon Ltd.). Neomycin-resistant ES cell colonies were isolated and expanded. Targeted ES cells were micro-injected into the blastocysts of C57BL/6 J female mice and transferred into the uteri of pseudo-pregnant mothers. Heterozygous mice were generated from mating of chimeric and C57BL/6 J mice. The heterozygous mice were crossed with Flp recombinant mice (003800, Jackson Lab) for deleting the neomycin-resistant elements. Then the Neo-deleted mice were crossed with EIIa-Cre mice (003314, Jackson Lab) for deleting the flox field and obtaining the conventional knockout mice. The heterozygous mice were then crossed with heterozygous mice to produce the homozygous knockout and control mice for experiments.

Immunoblotting

We obtained rabbit polyclonal antisera against human EMC10 as described previously (Wang et al., 2009). Here we purified the rabbit polyclonal antiserum to obtain the pure IgG against EMC10. We also prepared rabbit polyclonal antisera against human ATP1A4 (antigen peptides: CYDEIRKLLIRQHPDGWVERETYY). Protein expression was analyzed by immunoblotting as previously described (Zhou et al., 2015). Briefly, total protein extracts obtained from the tissues or spermatozoa were separated by electrophoresis on 12% (*w*/*v*) sodium dodecyl sulfate-polyacrylamide gels, transferred onto polyvinylidene fluoride membranes, and probed with primary antibodies as follows: EMC10 (1:5000 dilution); ATP1A1 (Proteintech, 1:5000 dilution); ATP1A4 (1:1000 dilution); ATP1B3 (Abcam, 1:1000 dilution); CFTR (Abcam, 1:1000 dilution); Tyrosine phosphorylation (clone 4G10, Millipore, 1:10000 dilution); β-actin and α-tubulin (Sigma, 1:200000 and 1:20000, respectively). The bound IgG was detected with goat-anti-rabbit (Sigma) or goat-anti-mouse (Millipore) antibody conjugated to horseradish peroxidase at a dilution of 1:10000. ECL Plus (Amersham) were used for chemiluminescence detection.

Sperm preparation

The weights of whole body, testis, and epididymis were measured, and spermatozoa from wild-type and null mice were obtained from the testis as well as the adult mouse caput, proximal corpus, distal corpus, and cauda epididymidis. Enriched Krebs–Ringer bicarbonate (EKRB) medium for mouse sperm capacitation was adopted from previously published reports (Zhou et al., 2015). The final composition of the medium was 120 mM NaCl, 4.8 mM KCl, 1.0 mM $CaCl_2$, 1.2 mM $MgSO_4$, 1.2 mM KH_2PO_4, 5 mM glucose, 21 mM sodium lactate, 0.25 mM sodium pyruvate, 25 mM $NaHCO_3$, and 3 mg/ml BSA. All the chemicals were purchased from Sigma and were of the highest purity available. In some experiments, medium without $NaHCO_3$ was derived by adding 25 mM NaCl instead of 25 mM $NaHCO_3$. In some experiments, Ca^{2+}-free media were used and the Ca^{2+} was added back to final concentrations if necessary. For morphological observation, sperm were fixed in 4% (*w*/*v*) paraformaldehyde for 30 min. To examine the motility and capacitation, sperm were incubated in the EKRB medium.

Immunofluorescence staining

Immunofluorescence was indirectly detected as described previously (Zhou et al., 2015). Ejaculated spermatozoa were either

provided by volunteers with proven fertility or collected from the cauda epididymidis of fertile adult mice. Spermatozoa were fixed in 4% (*w*/*v*) paraformaldehyde for 30 min at room temperature, and 1:100 diluted rabbit polyclonal antibody to EMC10 was applied. FITC-labeled goat-anti-rabbit IgG (Sigma) was used as the secondary antibody (1:200 dilution). Then sperm cells were counterstained with PI for identifying the cell nucleus or PNA-FITC (Sigma) for the acrosome if necessary. All the images were taken with a BX51 fluorescence microscope (Olympus).

Sperm motility analysis

The analysis procedure was a modification of our previously published method (Zhou et al., 2013). Sperm motility was assayed by using an HTM-TOX IVOS sperm motility analyzer (version 12.3 A, Hamilton-Thorn Research). The instrument settings were as follows: temperature, 37°C; minimum cell size, two pixels; minimum contrast, 50; minimum static contrast, 25; low VAP cutoff, 20.0; low VSL cutoff, 30.0; threshold straightness, 50%; static head size, 0.3–1.95; static head intensity, 0.5–1.3; magnification, 0.81. Thirty frames were acquired at a frame rate of 60 Hz. The playback feature was used during analysis to check the accuracy of the method.

Assessment of sperm chlortetracycline staining and fertilization

Spermatozoa were collected for staining with chlortetracycline (CTC) and assessing sperm capacitation and the acrosome reaction as described previously (Zhou et al., 2013). A total of at least 300 sperm cells were assessed for different CTC staining patterns: F, with uniform fluorescence over the entire head, characteristic of uncapacitated cells with intact acrosomes; B, with a fluorescence-free band in the postacrosomal region, characteristic of capacitated, acrosome-intact cells; AR, with dull or absent fluorescence over the sperm head, characteristic of capacitated, acrosome-reacted cells. Bright fluorescence was visible on the midpiece at all three stages. The methods for *in vitro* fertilization and ICSI in mice followed those described in our previous references (Gu et al., 2011; Zhou et al., 2013).

Proteomic expression profile analysis

Spermatozoa from 17 wild-type and 17 *Emc10*-null male mice at the age of 8–12 weeks were collected and pooled for protein extraction and digestion with trypsin. The resultant peptides were labeled with chemicals from the TMT 6-plex reagent kit (Pierce Biotechnology). Then the mixed and labeled peptides were fractionated by high pH separation using an Aquity UPLC system (Waters Corporation) and analyzed by a quadrupole-Orbitrap mass spectrometer (Q-Exactive) (Thermo Fisher Scientific). Data processing and quantification were handled by Proteome Discoverer software, Mascot, Scaffold Q+, as well as GO term enrichment analysis (http://david.abcc.ncifcrf.gov/) and IPA (http://www.ingenuity.com). Detailed descriptions for the proteomic analysis can be found in Supplementary material.

Measurement of intracellular Na^+, Ca^{2+}, and pH in spermatozoa

Spermatozoa were loaded with 20 μM SBFI-AM + 0.2% (*v*/*v*) pluronic acid for 60 min at 37°C and 5% (*v*/*v*) CO_2, and then washed twice and resuspended in EKRB medium devoid of BSA. The fluorescence signal from alternate excitation at 340 and 380 nm was recorded by using a luminescence spectrometer (BioTek), and the Na^+ concentration was calculated using the 340/380 ratio of fluorescence as described elsewhere (Torres-Flores et al., 2008). The methods for intracellular Ca^{2+} and pH in sperm followed those described in our previous references (Zhou et al., 2013, 2015).

Sperm preparation from asthenozoospermic patients

Ejaculated spermatozoa were obtained from asthenozoospermic patients and male controls. The study design was reviewed and approved by the ethical committee of the Huashan Hospital, Fudan Univeristy, and performed in accordance with the ethical standards laid down in the 1964 Declaration of Helsinki and its later amendments. A total of 27 patients were included between March 1 and April 30 in 2017. Subjects with anatomical abnormality of the reproductive system, untreated endocrine disorders, drug or alcohol abuse within the previous 2 years, or having habits that might affect the sperm motility were excluded.

Statistical analysis

The statistical significance of differences between samples from wild-type and knockout groups was analyzed by the Student's *t*-test by using SigmaPlot12.5 software. Statistical significance was defined as $P < 0.05$.

Supplementary material

Supplementary material is available at *Journal of Molecular Cell Biology* online.

Acknowledgements

The authors would like to thank Dr Trevor G. Cooper for reviewing and editing the manuscript. We also thank Dr Winnie Shum (School of Life Science and Technology, ShanghaiTech University) for assistance with light microscopy.

Funding

This work was supported by the National Basic Research Program (2014CB943103 to Y.Z., 2015CB943003 to Q.D.), the National Natural Science Foundation of China (31471104 and 31671203 to Y.Z., 81370753 to Q.D., 81070647 and 81370936 to X.W.). This work was also sponsored by grants from Shanghai Pujiang Program (16PJ1401700 to X.W.) and Science and Technology Commission of Shanghai Municipality (16140901200 to X.W.).

Conflict of interest: none declared.

Author contributions: Y.Z. and X.W. designed, performed, and analyzed most of the experiments in this study. F.W., M.Z., Q.Y., and Y.R. performed partial experiments. H.S., J.L., and Z.X.

provided samples or technical support. C.W.L. aided in the design of animal model. S.M., Y.L, X.C., and R.H. assisted X.W as well as F.W. with experiments. Y.Z. and Q.D. supervised the study. Y.Z., X.W., and Y.Z wrote the manuscript.

References

Abou-haila, A., and Tulsiani, D.R. (2009). Signal transduction pathways that regulate sperm capacitation and the acrosome reaction. Arch. Biochem. Biophys. *485*, 72–81.

Baker, M.A., Hetherington, L., and Aitken, R.J. (2006). Identification of SRC as a key PKA-stimulated tyrosine kinase involved in the capacitation-associated hyperactivation of murine spermatozoa. J. Cell Sci. *119*, 3182–3192.

Christianson, J.C., Olzmann, J.A., Shaler, T.A., et al. (2011). Defining human ERAD networks through an integrative mapping strategy. Nat. Cell Biol. *14*, 93–105.

Cooper, T.G., Yeung, C.H., Wagenfeld, A., et al. (2004). Mouse models of infertility due to swollen spermatozoa. Mol. Cell. Endocrinol. *216*, 55–63.

Darszon, A., Acevedo, J.J., Galindo, B.E., et al. (2006). Sperm channel diversity and functional multiplicity. Reproduction *131*, 977–988.

Gu, T.P., Guo, F., Yang, H., et al. (2011). The role of Tet3 DNA dioxygenase in epigenetic reprogramming by oocytes. Nature *477*, 606–610.

Harel, T., Yesil, G., Bayram, Y., et al. (2016). Monoallelic and biallelic variants in EMC1 identified in individuals with global developmental delay, hypotonia, scoliosis, and cerebellar atrophy. Am. J. Hum. Genet. *98*, 562–570.

Jimenez, T., McDermott, J.P., Sanchez, G., et al. (2011). Na,K-ATPase alpha4 isoform is essential for sperm fertility. Proc. Natl Acad. Sci. USA *108*, 644–649.

Jonikas, M.C., Collins, S.R., Denic, V., et al. (2009). Comprehensive characterization of genes required for protein folding in the endoplasmic reticulum. Science *323*, 1693–1697.

Junes-Gill, K.S., Gallaher, T.K., Gluzman-Poltorak, Z., et al. (2011). hHSS1: a novel secreted factor and suppressor of glioma growth located at chromosome 19q13.33. J. Neurooncol. *102*, 197–211.

Junes-Gill, K.S., Lawrence, C.E., Wheeler, C.J., et al. (2014). Human hematopoietic signal peptide-containing secreted 1 (hHSS1) modulates genes and pathways in glioma: implications for the regulation of tumorigenicity and angiogenesis. BMC Cancer *14*, 920.

Kaplan, J.H. (2002). Biochemistry of Na,K-ATPase. Annu. Rev. Biochem. *71*, 511–535.

Lahiri, S., Chao, J.T., Tavassoli, S., et al. (2014). A conserved endoplasmic reticulum membrane protein complex (EMC) facilitates phospholipid transfer from the ER to mitochondria. PLoS Biol. *12*, e1001969.

Li, Y., Zhao, Y., Hu, J., et al. (2013). A novel ER-localized transmembrane protein, EMC6, interacts with RAB5A and regulates cell autophagy. Autophagy *9*, 150–163.

Liu, P., Jenkins, N.A., and Copeland, N.G. (2003). A highly efficient recombineering-based method for generating conditional knockout mutations. Genome Res. *13*, 476–484.

Orgebin-Crist, M.C. (1967). Sperm maturation in rabbit epididymis. Nature *216*, 816–818.

Ren, D., Navarro, B., Perez, G., et al. (2001). A sperm ion channel required for sperm motility and male fertility. Nature *413*, 603–609.

Richard, M., Boulin, T., Robert, V.J., et al. (2013). Biosynthesis of ionotropic acetylcholine receptors requires the evolutionarily conserved ER membrane complex. Proc. Natl Acad. Sci. USA *110*, E1055–E1063.

Satoh, T., Ohba, A., Liu, Z., et al. (2015). dPob/EMC is essential for biosynthesis of rhodopsin and other multi-pass membrane proteins in Drosophila photoreceptors. eLife *4*, e06306.

Thompson, A., Schafer, J., Kuhn, K., et al. (2003). Tandem mass tags: a novel quantification strategy for comparative analysis of complex protein mixtures by MS/MS. Anal. Chem. *75*, 1895–1904.

Torres-Flores, V., Garcia-Sanchez, N.L., and Gonzalez-Martinez, M.T. (2008). Intracellular sodium increase induced by external calcium removal in human sperm. J. Androl. *29*, 63–69.

Ueno, S., Takeda, K., Noguchi, S., et al. (1997). Significance of the beta-subunit in the biogenesis of Na^+/K^+-ATPase. Biosci. Rep. *17*, 173–188.

Visconti, P.E., Bailey, J.L., Moore, G.D., et al. (1995a). Capacitation of mouse spermatozoa. I. Correlation between the capacitation state and protein tyrosine phosphorylation. Development *121*, 1129–1137.

Visconti, P.E., Moore, G.D., Bailey, J.L., et al. (1995b). Capacitation of mouse spermatozoa. II. Protein tyrosine phosphorylation and capacitation are regulated by a cAMP-dependent pathway. Development *121*, 1139–1150.

Wang, X., Gong, W., Liu, Y., et al. (2009). Molecular cloning of a novel secreted peptide, INM02, and regulation of its expression by glucose. J. Endocrinol. *202*, 355–364.

Wang, X.C., Xu, S.Y., Wu, X.Y., et al. (2004). Gene expression profiling in human insulinoma tissue: genes involved in the insulin secretion pathway and cloning of novel full-length cDNAs. Endocr. Relat. Cancer *11*, 295–303.

Wek, R.C., Jiang, H.Y., and Anthony, T.G. (2006). Coping with stress: eIF2 kinases and translational control. Biochem. Soc. Trans. *34*, 7–11.

Xu, B., Hsu, P.K., Stark, K.L., et al. (2013). Derepression of a neuronal inhibitor due to miRNA dysregulation in a schizophrenia-related microdeletion. Cell *152*, 262–275.

Xu, W.M., Shi, Q.X., Chen, W.Y., et al. (2007). Cystic fibrosis transmembrane conductance regulator is vital to sperm fertilizing capacity and male fertility. Proc. Natl Acad. Sci. USA *104*, 9816–9821.

Zeng, H.T., and Tulsiani, D.R. (2003). Calmodulin antagonists differentially affect capacitation-associated protein tyrosine phosphorylation of mouse sperm components. J. Cell Sci. *116*, 1981–1989.

Zhou, Y., Ru, Y., Shi, H., et al. (2015). Cholecystokinin receptors regulate sperm protein tyrosine phosphorylation via uptake of HCO_3^-. Reproduction *150*, 257–268.

Zhou, Y., Ru, Y., Wang, C., et al. (2013). Tripeptidyl peptidase II regulates sperm function by modulating intracellular Ca^{2+} stores via the ryanodine receptor. PLoS One *8*, e66634.